Chemical Science

ROYAL SOCIETY OF CHEMISTRY

EDGE ARTICLE

View Article Online
View Journal | View Issue

Cite this: *Chem. Sci.*, 2025, **16**, 21508

All publication charges for this article have been paid for by the Royal Society of Chemistry

Received 2nd July 2025
Accepted 28th September 2025

DOI: 10.1039/d5sc04870b

rsc.li/chemical-science

Tunable mechanics and energetics in structurally diverse TNPG-based metal organic networks

Shayan Karak, [ab] Soubhik Khata, [ab] Shamim Ahmad,[c] Abhishek Kumar Yadav, [d] Najla AlMasoud,[e] Taghrid S. Alomar,[e] Srinivas Dharavath, *[d] C. Malla Reddy *[c] and Rahul Banerjee *[abf]

Developing high-energy materials that are powerful yet safe requires a careful balance between thermal stability, mechanical strength, and detonation performance. While metal coordination is a known strategy to improve the thermal stability of energetic compounds like trinitrophloroglucinol (TNPG), mono-metallic networks often suffer from diminished detonation performance and increased sensitivity. This work introduces a new class of hetero-metallic metal–organic networks, MM′-TNPG (M/M′ = Li, Na, K), that harmonizes all critical performance parameters, including enhanced thermal stability, reduced sensitivity, and high detonation output. Particularly, we present the first systematic correlation between mechanical properties evaluated *via* nanoindentation and detonation performance, revealing how structural features and metal coordination govern the material's robustness and energetic behavior. Correlating mechanical properties with the detonation and safety parameters could potentially offer a predictive approach to designing safer designs of high-performance, energetic materials. The hetero-metallic systems exhibit synergistic enhancement in mechanical strength without compromising explosive efficiency. This work introduces a novel design strategy for safer, high-performance, energetic materials, establishing a vital structural–mechanical–energetic property relationship that has previously been unexplored in this field.

Introduction

High-energy materials are indispensable in propulsion, mining, and defense.[1,2] Yet their practical application is often constrained by poor thermal stability and high sensitivity to mechanical stimuli.[3–5] While significant attention has been devoted to enhancing thermal stability and detonation performance, the mechanical behavior of these materials, equally critical for safety, processability, and operational reliability, remains underexplored. Mechanical instability can lead to microcracks or structural failure under stress, increasing the risk of accidental ignition or uncontrolled detonation.[6,7] Therefore, a deeper understanding of mechanical response, especially at the nanoscale, is essential to advance the safe design of next-generation energetic materials. TNPG, a nitro-aromatic compound featuring three nitro and three hydroxyl groups, is a highly energetic molecule due to its excellent detonation characteristics.[8–13] However, intrinsic thermal instability and high sensitivity hindered its practical applicability. Achieving a balance between detonation efficiency, thermal robustness, and mechanical resilience is the key to realizing TNPG's potential in practical applications.[14–17]

Metal coordination has emerged as a promising strategy to stabilize energetic molecules like TNPG by increasing structural rigidity.[18–22] While this approach is known to enhance thermal stability, it often comes with trade-offs, such as reduced detonation efficiency and increased sensitivity. Previous reports on metal-coordinated energetic frameworks are largely limited to mono-metallic systems, which tend to prioritize one property at the expense of others. The influence of metal-ion choice, framework dimensionality, and coordination geometry on the combined mechanical and energetic behavior remains poorly understood.

In this work, we address this gap by presenting the first comprehensive investigation into mono- and hetero-metallic TNPG-based metal–organic networks, M-TNPG and MM′-TNPG (M/M′ = Li, Na, K), with a focus on correlating their structures → mechanical properties → energetic performances. These materials were synthesized using thermo-evaporative *in situ* crystallization in water, which directly

[a]*Department of Chemical Sciences, Indian Institute of Science Education and Research Kolkata, West Bengal-741246, India. E-mail: r.banerjee@iiserkol.ac.in*

[b]*Centre for Advanced Functional Materials, Indian Institute of Science Education and Research, Kolkata, Mohanpur 741246, India*

[c]*Department of Chemistry, IIT Hyderabad, Telangana-502329, India. E-mail: cmallareddy@gmail.com*

[d]*Energetic Materials Laboratory, Department of Chemistry, Indian Institute of Technology Kanpur, Kanpur, Uttar Pradesh 208016, India. E-mail: srinivasd@iitk.ac.in*

[e]*Department of Chemistry, College of Science, Princess Nourah bint Abdulrahman University, P.O. Box 84427, Riyadh, Saudi Arabia*

[f]*College of Science, Korea University, 145 Anam-ro Seongbuk-gu, South Korea*

yields single crystals suitable for structural elucidation, offering a rapid, scalable route to bulk materials.

Results and discussion

Synthetic procedures

General procedure for synthesis. To investigate the structural diversity and functional potential of alkali metal coordination with 2,4,6-trinitrobenzene-1,3,5-triol (TNPG), we synthesized a series of metal–organic architectures involving mono- and hetero-metallic combinations of Li^+, Na^+, and K^+ (Fig. 1a–d). TNPG, bearing three hydroxyl and three nitro groups on a benzene core, offers multiple coordination sites, making it an ideal platform to explore ion-mediated coordination network evolution. The synthesis of M-TNPG coordination networks was carried out by mixing an aqueous solution of the metal hydroxide (MOH, 1.2 mmol) with a solution of TNPG (0.4 mmol) in water (Section S1). The resulting reaction mixture was

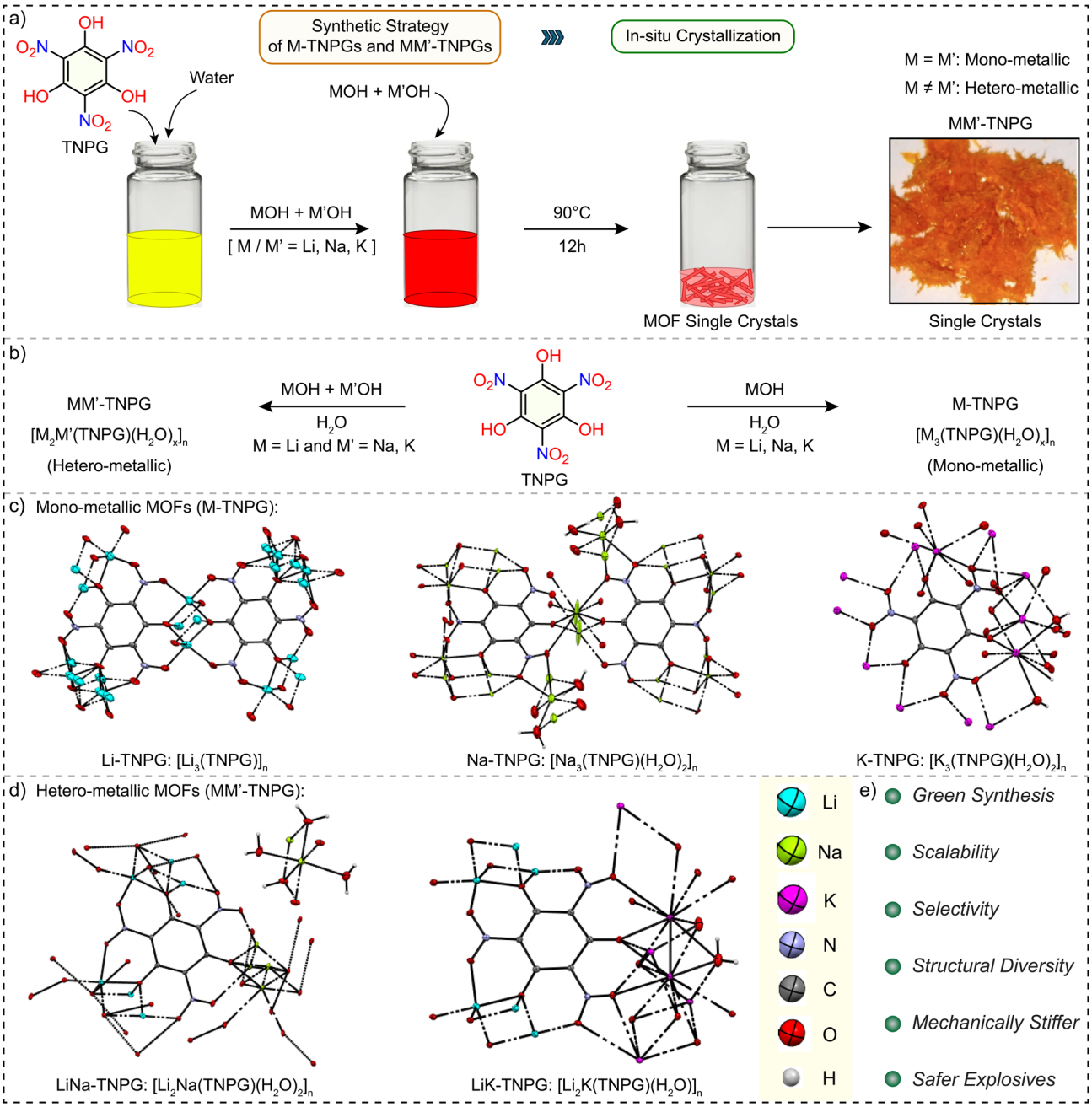

Fig. 1 (a) Schematic representation of the synthetic methodologies and (b) general synthetic scheme of M-TNPGs and MM′-TNPGs (M/M′ = Li, Na, and K). Single crystal X-ray diffraction structure of the (c) mono-metallic metal–organic networks (M-TNPGs: M = Li, Na, and K) and (d) hetero-metallic metal–organic networks (MM′-TNPG: MM′ = LiNa and LiK). (e) Synthetic advantages and properties of the metal–organic networks.

subjected to ultrasonication for ~2 minutes. The mixture was then placed in a hot air oven operating at 90 °C for 12 hours. During this time, the water evaporated slowly, leading to the formation of a supersaturated solution of M-TNPG, which precipitated out as single crystals (Fig. 1a and b). After crystallization, the crystals were isolated from the solution, washed with cold water, followed by acetone, and dried under vacuum at 60 °C for ~4 hours to yield the pure M-TNPG coordination architectures. The hetero-metallic coordination networks, LiNa-TNPG and LiK-TNPG, were synthesized using a similar methodology (Section S1). The same steps as described for M-TNPG synthesis were followed, with the addition of both LiOH and NaOH (or KOH) (1.2 mmol of each) in equimolar ratio to the TNPG (0.4 mmol) solution enabling the formation of the respective hetero-metallic networks. These hetero-metallic networks were purified and characterized following the same procedures as the M-TNPGs (Fig. 1a and b).

The general chemical formula of M-TNPG can be represented as $[M_3(TNPG)(H_2O)_x]_n$, where x represents the number of coordinated water molecules in the asymmetric unit (Fig. 1b). Specifically, the formulae for Li-TNPG, Na-TNPG, and K-TNPG are $[Li_3(TNPG)]_n$, $[Na_3(TNPG)(H_2O)_2]_n$, and $[K_3(TNPG)(H_2O)_2]_n$, respectively (Fig. 1c and Table S3). The general chemical formula of MM′-TNPG is $[M_2M'(TNPG)(H_2O)_x]_n$, where M = Li and M′ = Na or K for LiNa-TNPG and LiK-TNPG, respectively (Fig. 1b). The exact formulae are $[Li_2Na(TNPG)(H_2O)_2]_n$ for LiNa-TNPG and $[Li_2K(TNPG)(H_2O)]_n$ for LiK-TNPG (Fig. 1d and Table S3).

Characterization

Structural elucidation through single crystal X-ray diffraction. Crystallization of TNPG in water yields block-shaped single crystals, adopting a trigonal system (space group: *P*-3*c*1).[14] The X-ray structure reveals that two nitro groups lie nearly in the same plane of the aromatic ring and form intramolecular hydrogen bonds (Section S7 and Table S4) with adjacent hydroxyl groups, while the third nitro group is twisted out of plane (~62.2°) to minimize steric repulsion (Fig. S38). SCXRD analysis revealed distinct architectures among the mono-metallic networks. Li-TNPG crystallizes in the *P*-1 space group, forming a 2D network-like structure with a ladder growth in the a-direction (Fig. 2a). Each Li^+ ion adopts a distorted square pyramidal geometry, coordinating with three phenolic oxygens and two $-NO_2$ oxygens from adjacent TNPG units (Fig. 2a). The relatively small ionic radius and high charge density of Li^+ favor compact, directional bonding, resulting in a tightly packed 2D motif with minimal interstitial space, with a void volume of ~181 Å^3 (Fig. S39).[16] In the crystal structure of Li-TNPG the void space is occupied by the lattice water molecules (Fig. S35). The strong π···π stacking (dπ···π = ~3.4 Å) between the phenyl rings further stabilizes the Li-TNPG lattice (Fig. S37). Na-TNPG, by contrast, adopts an orthorhombic *Pba*2 space group and displays a similar structure to Li-TNPG (Fig. 2b). Here, Na^+ ions exhibit distorted cubic and mono-capped trigonal prismatic coordination geometries involving both phenolic and $-NO_2$ oxygen donors (Fig. 2b). The extended connectivity among TNPG ligands and the flexible coordination sphere of Na^+ facilitates the formation of a dense 2D network with zero void volume (Fig. S40). The closely packed 2D network, Na-TNPG, is further stabilized by strong π···π stacking interactions (dπ···π = ~3.4 Å) between the phenyl rings and reinforces the architecture's overall stability (Fig. S37). K-TNPG crystallizes in the chiral $P3_1$ space group, forming a 3D structure.[23,24]

K^+ ions are deca-coordinated, adopting a distorted bi-capped square antiprismatic geometry (Fig. 2c). Their larger ionic radius promotes multidirectional bonding with oxygen atoms from multiple TNPG ligands, culminating in a densely packed 3D network. Notably, the phenyl rings engage in significant π··· π stacking interactions (dπ···π = ~3.5 Å), akin to its lithium and sodium analogs, which further reinforce the stability (Fig. S37). It is also noted that one of the K^+ is also involved in weak interaction with the ring carbon of TNPG, resulting in tilted ring geometry with a torsional angle (φ) of ~19° (Fig. S37).

To further tune the geometry of the coordination network and explore the synergistic metal–ligand interactions, we synthesized hetero-metallic analogs: LiNa-TNPG and LiK-TNPG (Fig. 1d). An intriguing aspect is the observed selectivity in hetero-metallic network formation. Attempts to generate NaK-TNPG reproducibly yielded only K-TNPG, while ternary mixtures containing Li^+, Na^+, and K^+ (in equimolar ratio) resulted exclusively in LiK-TNPG, with Na^+ selectively excluded. This selectivity is driven by the strong affinity of Li^+ for the hard phenolate oxygens of TNPG, which modulates the ligand's electronic environment and favors subsequent coordination with softer cations like K^+ over Na^+. LiNa-TNPG crystallizes in the orthorhombic $P2_12_12$ space group and represents a superlattice-like network where Li^+ and Na^+ are co-coordinated with TNPG (Fig. 3a). This mixed-metal coordination not only introduces heterogeneity at the local bonding level but also fosters an ordered one-dimensional $[Na(OH_2)_2]_n$ chain running through the hexagonal pores formed by the LiNa–TNPG substructure (Fig. 3a). The overall effect is a composite network that merges the directional binding character of Li^+ with the more flexible and pore-promoting nature of Na^+. The formation of a superlattice-like network in LiNa-TNPG makes the network very compact with no void volume, unlike their individual mono-metallic networks (Li-TNPG and Na-TNPG). LiK-TNPG, on the other hand, crystallizes in the monoclinic $P2_1/c$ space group, its formation occurs selectively in the presence of both Li^+ and K^+, underscoring a preferential stabilization over the potential NaK analog (Fig. 1d). Structural analysis indicates that Li^+ plays a key role in templating the TNPG backbone, while the bulky K^+ ions are anchored *via* multidentate coordination, resulting in a compact, reinforced 3D network. The multidentate coordination ability of K^+ generates the rigid hetero-metallic LiK-TNPG with zero void volume (Fig. S42). Akin to the mono-metallic coordination networks, strong π···π (dπ···π = ~3.4 Å) interactions also contribute to the overall stability of the hetero-metallic architecture (Fig. S37). Topologically, the Na-TNPG, Li-TNPG, and LiNa-TNPG metal–organic networks are related to the rod-packed *dum* net, which is homotopic to the 2D *hcb* net.[25]

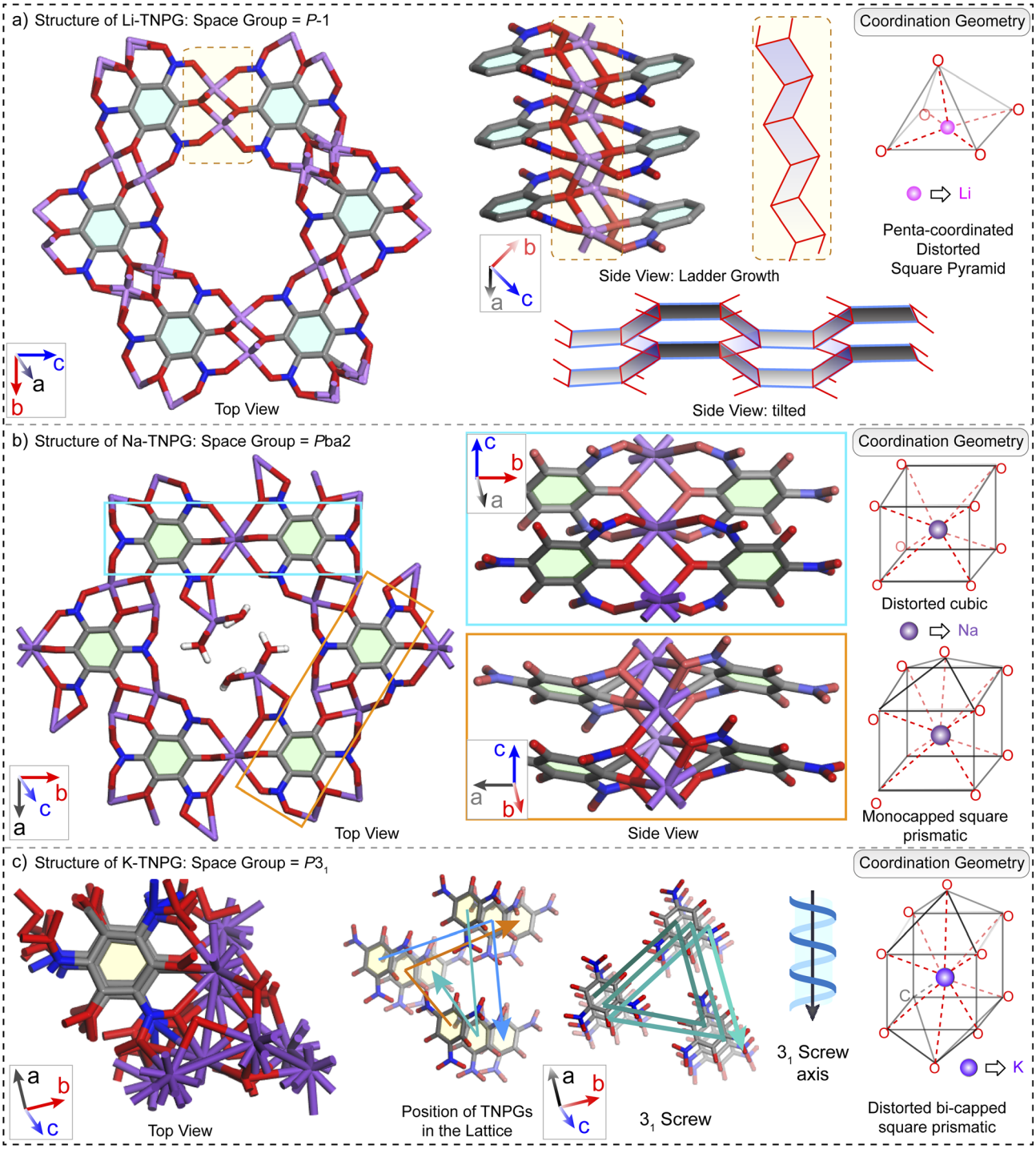

Fig. 2 Single crystal X-ray diffraction structures of M-TNPGs (M = Li, Na, and K) from top and side view and the coordination geometries of M^+ ions: (a) Li-TNPG, (b) Na-TNPG, and (c) K-TNPG.

Bulk purity and chemical stability. The purity of all as-synthesized TNPG-based mono- and hetero-metallic coordination networks (M-TNPGs and MM′-TNPGs) was evaluated using powder X-ray diffraction (PXRD) and Fourier-transform infrared (FT-IR) spectroscopic techniques (Fig. 3c and S5). The PXRD patterns of samples show agreement, confirming that the synthetic methodology consistently yields structurally identical materials (Section S3). Furthermore, the experimental PXRD profiles match closely with simulated patterns derived from single-crystal X-ray diffraction (SCXRD) data, strongly affirming the phase purity and structural integrity of the compounds, where minor structural inconsistencies can lead to unpredictable or unsafe detonation behavior. Furthermore, the Pawley refinement of the Li-TNPG displayed good agreement between

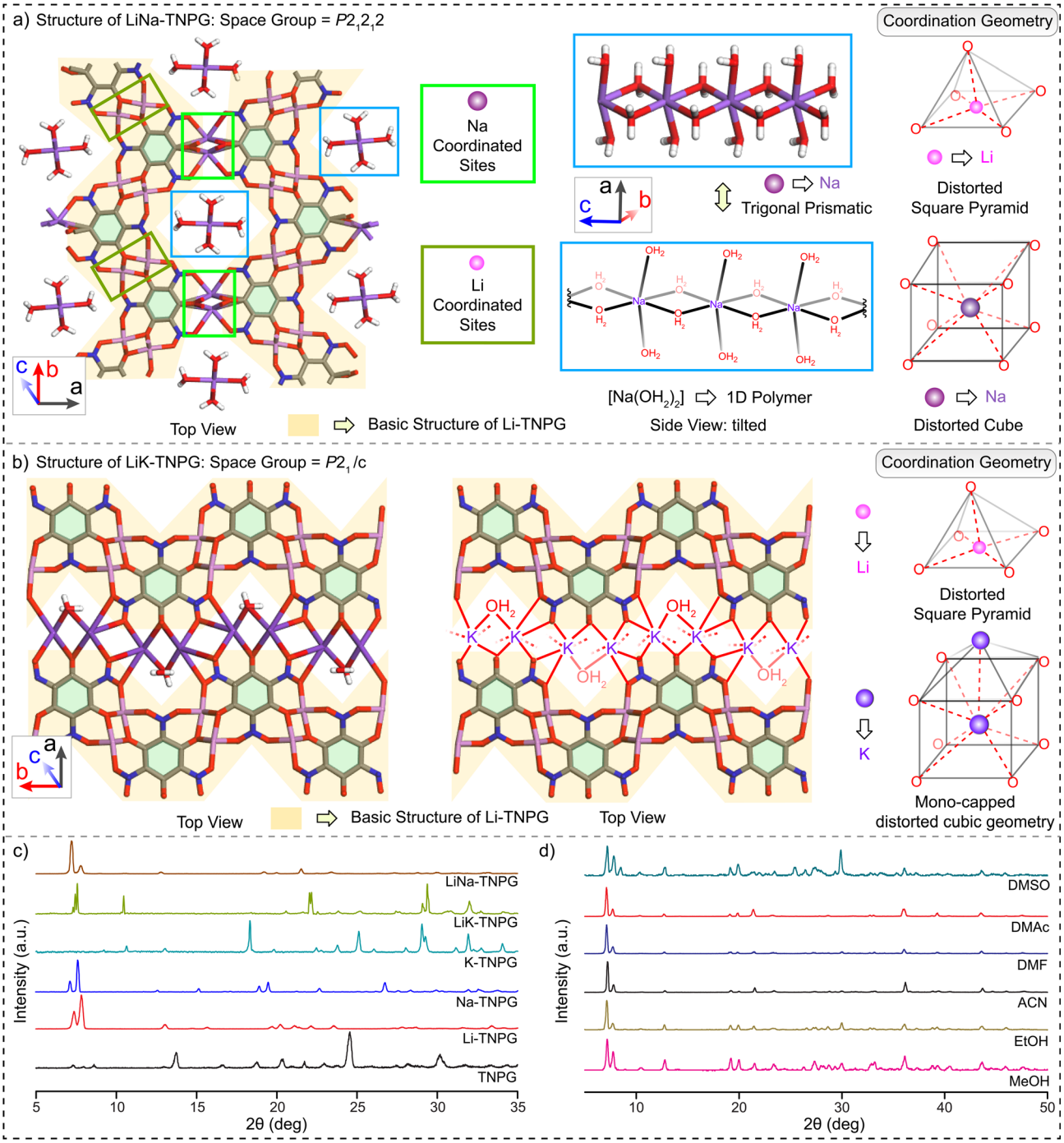

Fig. 3 Single crystal X-ray diffraction structures of MM′-TNPGs and the coordination geometries of M^+ ions: (a) LiNa-TNPG and (b) LiK-TNPG. (c) and (d) Powder X-ray diffraction patterns of as-synthesized M-TNPGs (M = Li, Na, and K) and MM′-TNPGs (MM′ = LiK and LiNa) following thermo-evaporative *in situ* crystallization and (d) LiNa-TNPG after treatment with solvents with a high dielectric constant ranging from ~24 to 47.

experimental and simulated PXRD patterns, further confirming the phase purity (Fig. S7–9). In addition to structural uniformity, the chemical stability of the M-TNPG and MM′-TNPG metal–organic networks was probed by exposing them to a series of solvents with varying dielectric constants, ranging from low (methanol: 32.7, ethanol: 24.3) to high (acetonitrile: 37.5, DMF: 36.71, DMAc: 37.78, DMSO: 46.70). PXRD analyses conducted after solvent exposure reveal that all the architectures retain their crystallinity and structural features in the presence of most solvents, including high-dielectric media such as DMF and DMAc, underscoring their chemical stability (Fig. 3d and S10–14). However, partial degradation was observed upon treatment with DMSO, indicating a limitation under strongly solvating conditions.

Mechanical properties. Nanoindentation has emerged as a widely adopted method for assessing the mechanical

properties of molecular single crystals (SCs),[26–31] though its use in coordination networks, especially those containing alkali metals, remains relatively limited.[20,32,33] We envisaged that measuring nanoindentation responses in high-energy materials can offer valuable insights into their mechanical impact sensitivity parameter, yet this approach remains virtually unexplored. To bridge this gap, we present the first systematic investigation of nano-mechanical behavior in single crystals of TNPG and its mono- and hetero-metallic coordination networks, which can directly be correlated with impact and friction sensitivity.

TNPG crystallizes in a rhombohedral *P*-3*c*1 space group, forming a compact 3D molecular lattice. When probed along the (2–10) crystallographic face, these crystals displayed surprisingly high mechanical stiffness for a non-metal-coordinated system, with an average elastic modulus (E) of 21.21 ± 2.22 GPa and hardness (H) of 518.46 ± 95.66 MPa (Fig. 4a, S17, and Table S1). This resilience is likely driven by the presence of strong hydrogen-bonding networks (Fig. S34 and Table S4) despite the lack of coordination crosslinking. Upon the introduction of alkali metals, the mechanical responses varied substantially based on the metal ion and its coordination behavior. Among the mono-metallic networks, Li-TNPG exhibited the highest stiffness (E = 24.14 ± 3.23 GPa), although its hardness (H = 446.38 ± 113.89 MPa) was slightly lower relative to TNPG (Fig. 4j–l, S18, and S23). The higher

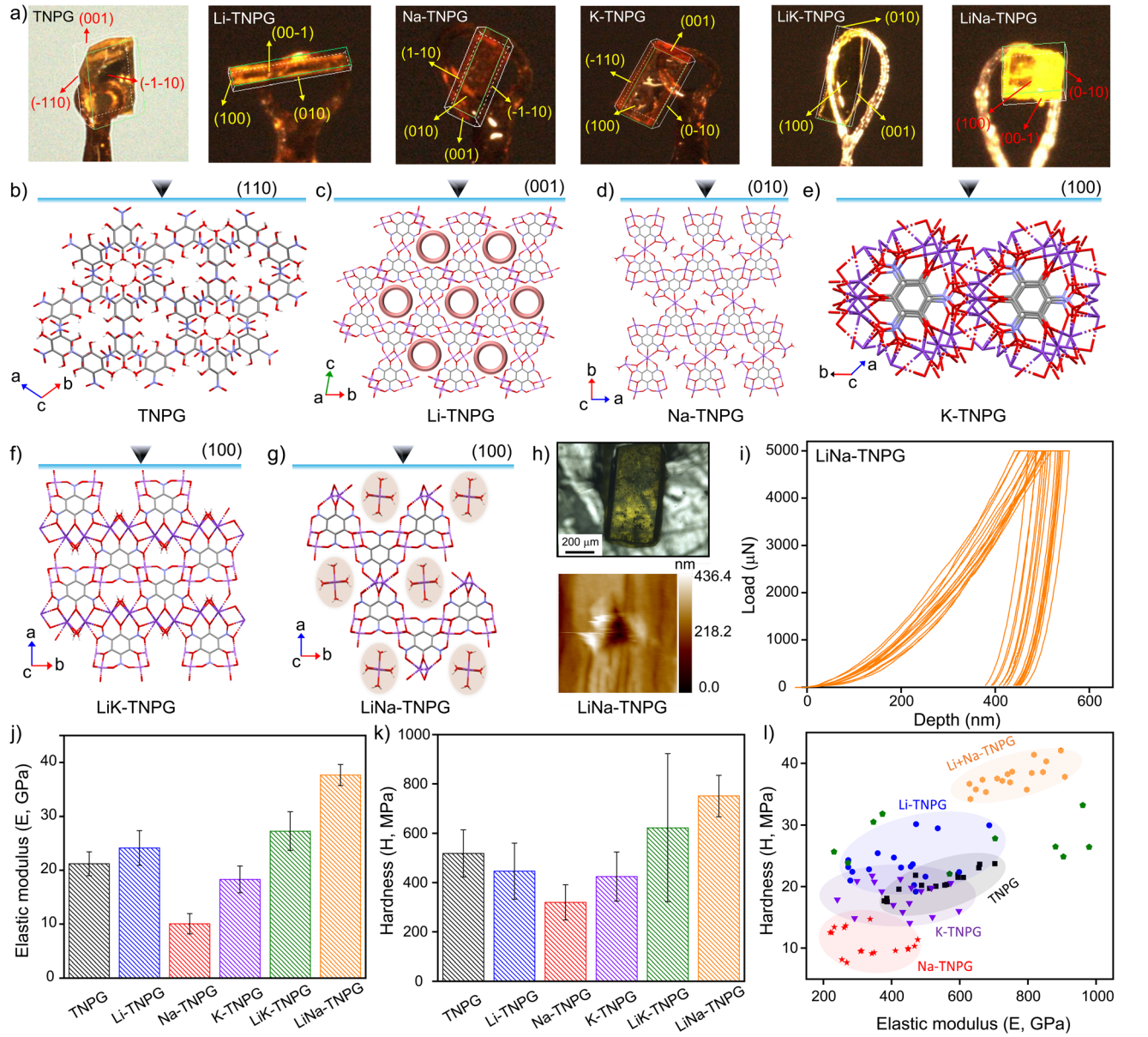

Fig. 4 (a) Images of the indexed faces of the single crystals (left to right: TNPG to LiNa-TNPG). (b–g) Crystal packing diagrams, showing the indenting faces of TNPG, M-TNPG (M = Li, Na, and K), and MM′-TNPG (MM′ = LiK and LiK). (h) An indented crystal and the SPM image after nanoindentation of LiNa-TNPG. (i) Load *vs.* depth profiles of indents from LiNa-TNPG. Average (j) elastic modulus and (k) hardness values. (l) The scattered plot of hardness *vs.* elastic modulus was obtained from a large number of indents from each sample.

elastic modulus is likely attributable to the formation of a 2D coordination network with strong Li–O links, which imparts increased stiffness along specific crystallographic axes. Indenting on the Na-TNPG SC revealed the softer nature of the network. Na-TNPG exhibits the lowest values for both elastic modulus (10.06 ± 1.89 GPa) and hardness (319.60 ± 71.56 MPa) among the three mono-metallic MOFs, accompanied by the deepest contact depth (h_c = 782.22 ± 84.60 nm) (Fig. 4j–l, S19, and S23). This reduction in mechanical stiffness could be attributed to the relatively weaker Na–O bonds supported by the lower charge density on Na^+ than on Li^+. K-TNPG occupied an intermediate position in terms of nano-mechanical properties, recording an elastic modulus of 18.30 ± 2.49 GPa and hardness of 424.54 ± 99.77 MPa (Fig. 4j–l, S20, and S23). The 3D network supported by K^+ ions, having higher coordination numbers than both Li^+ and K^+, offers greater rigidity than Na-TNPG. In contrast, a comparatively lower charge density of K^+ yields slightly reduced stiffness compared to the Li-TNPG due to a weaker coordination bond strength towards oxygen than Li^+. The nanoindentation studies on the mono-metallic system revealed that mechanical stiffness is a factor of the strength of coordination bonds, determined by their relative charge density, and the nature of metal–organic architecture, governed by coordination numbers of the metal ions. These two competitive factors create a non-linear structure–mechanical property correlation in the case of mono-metallic coordination networks (M-TNPGs).

To overcome these inherent limitations of mono-metallic frameworks, we turned to hetero-metallic systems that combine distinct ionic characteristics. Both LiK-TNPG and LiNa-TNPG demonstrated significantly enhanced mechanical properties, underscoring the cooperative effect of mixed-metal coordination (Fig. 3a and b, 4j–l, and Table S1). Among all tested materials, LiNa-TNPG exhibited the highest mechanical stiffness, with an elastic modulus of 37.65 ± 1.95 GPa and hardness of 751.00 ± 83.46 MPa (Fig. 4g–l, and S22). Its superlattice-like architecture features TNPG ligands bridging both Li^+ and Na^+ ions to generate a robust architecture, with embedded 1D $[Na(OH_2)_2]_n$ chains running through the voids (Fig. 3a and S43). The mechanical superiority of this material is attributed to a combination of strong Li–O and Na–O bonding, high architectural density, and reinforced internal packing. LiK-TNPG also showed enhanced stiffness (E = 25.60 ± 2.30 GPa) and a moderately higher hardness of 585.30 ± 89.20 MPa (Fig. 4j–l and S21). Its architecture consists of alternating layers of Li^+ and K^+ coordination propagating along the *c*-axis, which likely contributes to its improved load-bearing capacity (Fig. 3b). However, this system exhibited relatively higher data variability, potentially due to microfractures on the crystal surface introduced during sample drying (Fig. S21 and S23).

These results demonstrate that the nano-mechanical behavior of TNPG-based coordination networks can be finely tuned through targeted metal selection. The introduction of multiple alkali metal ions facilitates improved crosslinking and rigidity, leading to the enhancement of mechanical stability not only to the parent ligand molecule, TNPG, but also to surpass their mono-metallic networks (M-TNPGs). Both the factors, charge density on the metal ions, which determine the relative strengths of the coordination bonds, and coordination geometries are now determined synergistically from the combined effect of two different metal-ions involved in the hetero-metallic network.

Energetic properties. The physicochemical and energetic properties of TNPG-based metal–organic architectures, including density, heat of formation, thermal stability, detonation performance, and mechanical sensitivity, were thoroughly investigated, and the results are presented in Table S2. Thermal stability was assessed *via* thermogravimetric analysis and differential scanning calorimetry (TGA-DSC), ranging from 262 to 344 °C (Fig. 5d and S24–32). All TNPG-based metal–organic architectures, except K-TNPG (262 °C), exhibited excellent thermal stability with decomposition temperatures exceeding 318 °C, surpassing those of commonly used secondary explosives such as HMX (~279 °C) and HNS (~318 °C). In the case of the hetero-metallic coordination networks, minor weight loss below 100 °C arises from adsorbed water, while the subsequent loss between 100 °C and 200 °C is attributed to the release of coordinated water molecules prior to the thermal detonation event (Fig. S30 and 31). The heats of formation were experimentally determined using bomb calorimetry and ranged from −1244.10 to −2750.95 KJ mol^{-1}, with detailed data provided in the SI (Section S7 and Table S2). Densities were measured with a gas pycnometer in a helium atmosphere at 25 °C, revealing higher densities of all the coordination networks (ranging between 1.93 and 2.14 g cm^{-3}), presented in this study, than the parent ligand TNPG (1.89 g cm^{-3}) (Fig. 5c, and Table S2). The higher density is likely due to strong metal–ligand coordination and compact 2D and 3D network formation with minimum void volume. Based on experimental densities and heats of formation, the detonation parameters, such as velocity of detonation (VOD) and detonation pressure (DP), were calculated using Explo-5 software (version 7.01.01).

TNPG exhibited high detonation metrics (DP = 26.2 GPa; VOD = 8028 m s^{-1}) but suffered from poor thermal stability (T_{dec} = 155 °C), limiting its practical application. Coordination with Li^+ substantially improved thermal stability (T_{dec} = 344 °C), though detonation performance was reduced significantly (DP = 17.4 GPa; VOD = 7053 m s^{-1}). The overstabilization of the Li-TNPG coordination network due to the favourable hard–hard Li–O coordination bonding, as reflected by the highest heat of formation value, suppresses its energetic performance (Fig. 5e and f). As Na^+ has a moderate charge density, Na-TNPG shows a good balance between the detonation performance and thermal stability among the mono-metallic coordination networks. K^+, having the lowest charge density and larger size, exhibits inefficient coordination bonding with oxygens; K-TNPG exhibits the lowest thermal stability among the M-TNPGs. Additionally, in the dense 3D networks of K-TNPG, K^+ contributed to the dead weight, leading to inferior detonation performance (Fig. 5f and Table S2). Improving both the concerned properties, thermal stability and detonation velocity, has proven to be challenging by simply coordinating TNPG with a single alkali-metal ion.

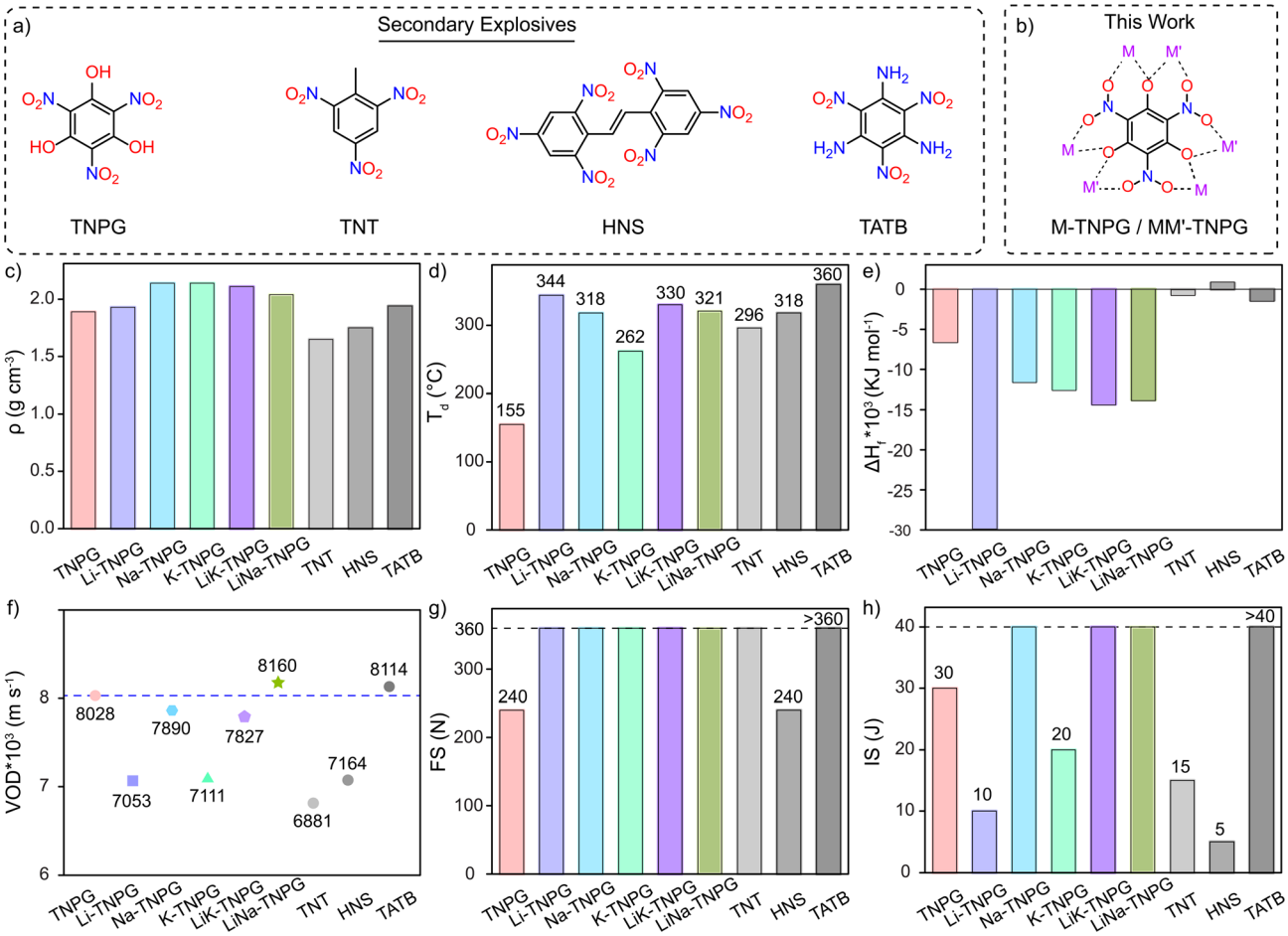

Fig. 5 (a) Literature reported secondary explosives.[34] (b) Strategy adopted in designing the secondary explosives in this work. The physico-chemical properties of the TNPG-based mono- and hetero-metallic coordination networks compared with the literature reported explosives: (c) Experimental density, (d) onset decomposition temperature, (e) heat of formation, (f) velocity of detonation (VOD), (g) friction, and (h) impact sensitivity.

Both hetero-metallic networks exhibited superior detonation performance when benchmarked against TNPG and their mono-metallic counterparts. LiNa-TNPG achieved a detonation pressure of 25.5 GPa and velocity of 8160 m s^{-1}, surpassing TNPG as well as both the Li- and Na-TNPG despite having a larger unit cell (Fig. S33). Nanoindentation and structural data suggest that LiNa-TNPG exhibits the highest mechanical stiffness, resisting deformation, which correlates with its high detonation pressure (DP). Such robust networks localize and direct energy release, enhancing the efficiency of detonation. This enhancement is attributed to dense metal coordination, mechanical rigidity, and minimal porosity, enabling more efficient energy propagation. Notably, LiNa-TNPG, owing to its unique structural features, exhibits the best performance among the five TNPG-based mono- and hetero-metallic coordination networks, demonstrating similar performance to the well-known heat-resistant explosive TATB (Fig. 5f). LiK-TNPG also demonstrated improved detonation metrics (DP = 23.6 GPa; VOD = 7827 m s^{-1}), outperforming both of their mono-metallic analogs (Li-TNPG and K-TNPG).

Impact and friction sensitivities were evaluated using the standard BAM fall hammer and friction tester. TNPG has a moderate sensitivity to mechanical stimuli (IS = 30 J and FS = 240 N) (Fig. 5g and h). The metal-coordination improved the friction sensitivity from 240 N in TNPG to 360 N in all the coordination networks, independent of the metal ion used and the structure of the networks (Fig. 5g). The Li^+ coordination, though, improves the thermal stability, but it is compromised by the impact sensitivity (IS = 10 J) along with the detonation matrices (Fig. 5f and h). Among the mono-metallic coordination networks (M-TNPGs), Na-TNPG provides a good balance between thermal stability, detonation, and sensitivities to mechanical stimuli (Fig. 5d and f–h). K-TNPG possesses poor detonation metrics and impact sensitivity with relatively low thermal stability, not sufficient to behave as a secondary explosive (Fig. 5d and h). So, it can be inferred that M-TNPGs, with homogeneous metal content, cannot provide the required balance among the mechanical, thermal, and energetic properties.

In contrast, hetero-metallic networks, already proven to be mechanically rigid, as depicted by nanoindentation studies, demonstrate excellent energetic performances (Fig. 4h–l and 5c–h). The high nano-mechanical stability also reflected their impact sensitivity parameters with an IS of 40 J, significantly

less sensitive than TNPG and HNS (IS = 5 J) (Fig. 5g–h).[21] Owing to their unique structural features, the hetero-metallic coordination networks exhibit high mechanical strength, reduced sensitivity, and high detonation efficiency. The presence of two different metal centers (Li^+ and Na^+) introduces heterogeneous bonding environments, leading to synergistic structural stabilization. This leads to reduced structural defects and better energy dissipation upon mechanical shock, hence, improved impact resistance. The best performance of LiNa-TNPG can be attributed to the presence of the 1D $[Na(OH_2)_2]_n$ chain embedded within its hexagonal pores. This chain likely reinforces architectural stability *via* additional H-bonding and electrostatic interactions, enhancing both mechanical rigidity and energetic performance. The nano-mechanical stiffness, measured by nanoindentation on the coordination network single crystals, cannot be linearly correlated with the detonation performance and impact sensitivity in the case of mono-metallic networks, as several deciding factors act in opposite directions. But, the correlation between mechanical properties and detonation performance is evident in the case of the hetero-metallic metal–organic networks: networks exhibiting higher mechanical stiffness also show improved detonation pressures and velocity, consistent with more efficient shockwave transmission and energy release. It is noteworthy that the nano-mechanical stiffness of the energetic material is not only crucial for resisting mechanical stimuli but also essential for determining the efficient shockwave transmission, restricting a material from premature decomposition, leading to the exploration of the full potential. The assessment of the nano-mechanical properties of the energetic materials *via* nano-indentation could potentially be correlated with their detonation performance. The high density, exceptional thermal stability, balanced energetic performance, and low mechanical sensitivity of the TNPG-based hetero-metallic coordination networks highlight their potential as promising alternatives to currently used secondary explosives such as TNT and HNS.[21]

Caution: These TNPG-based materials are highly energetic and must be handled under solvent-immersed conditions to prevent accidental initiation. Grinding should only be performed with ~100 μL of distilled water or ethanol to minimize frictional impact risks. Uncontrolled heating must be strictly avoided.

Conclusions

In summary, this study introduces a novel strategy for the design of safer, high-performance, energetic materials by integrating straightforward synthesis, structural engineering, and mechanical property evaluation. We demonstrate that nanoindentation, a technique traditionally underutilized in energetic materials, offers a powerful approach to assess insights into the mechanical stiffness and hardness, along with detonation behavior. The rational design of hetero-metallic TNPG-based coordination networks reveals a unique balance between thermal stability, mechanical robustness, and detonation performance. These hybrid networks outperform their mono-metallic counterparts by leveraging complementary metal–ligand interactions and structural densification. LiNa-TNPG, the most efficient metal–organic network, could be a promising candidate as a potential replacement for widely used secondary explosives such as TNT and HNS. The insights from this study not only expand the toolbox for highly energetic material development but also underscore the importance of mechanical properties, often overlooked, in guiding the next generation of high-performance energetic metal–organic architectures.

Author contributions

S. Karak and R. B. conceived the idea of the project. S. Karak and S. Khata synthesised and characterised the metal–organic networks. S. A. and C. M. R. performed the nanoindentation measurements. A. K. Y. and S. D. measured the energetic performance. N. A. and T. S. A. helped with the data analysis. The manuscript was written with contributions from S. Karak and R. B. All authors have given approval to the final version of the manuscript.

Conflicts of interest

There are no conflicts to declare.

Data availability

The data supporting this article have been included as part of the Supplementary Information (SI). The authors have cited additional references within the SI.[35–38]

CCDC 2401613, 2449186, 2449189, 2449198, 2449208, 2449429, 2483913, and 2484895 contain the supplementary crystallographic data for this paper.[39a–h]

Supplementary information: the crystallographic details can also be found in Table S3 (Section S7, SI). See DOI: **https://doi.org/10.1039/d5sc04870b**.

Acknowledgements

S. Karak acknowledges IISER Kolkata and PMRF (PMRF ID: 0501558) for the research fellowship (SRF), and S. Khata acknowledges UGC for the Research fellowship. A. K. Y. acknowledges IIT Kanpur for the FARE fellowship. S. D. acknowledges the core research grant (CRG/2023/000007), Science and Engineering Research Board, Department of Science and Technology, India, for funding. R. B. acknowledges IISER Kolkata for funding. The authors extend their appreciation to the Deanship of Scientific Research and Libraries at Princess Nourah bint Abdulrahman University for funding this work through the Visiting Researcher Program VR-45-004.

Notes and references

1 Q. Zhang and J. n. M. Shreeve, *Chem. Rev.*, 2014, **114**, 10527–10574.
2 O. S. Bushuyev, P. Brown, A. Maiti, R. H. Gee, G. R. Peterson, B. L. Weeks and L. J. Hope-Weeks, *J. Am. Chem. Soc.*, 2012, **134**, 1422–1425.

3 H. Xia, W. Zhang, Y. Jin, S. Song, K. Wang and Q. Zhang, *ACS Appl. Mater. Interfaces*, 2019, **11**, 45914–45921.
4 A. K. Yadav, V. D. Ghule and S. Dharavath, *Chem. Commun.*, 2025, **61**, 6901–6904.
5 Y. Bi, J. Tao, Y. Wu, L. Li, Y. Xu, E. Hu, B. Wu, J. Hu, C. Wang, J.-G. Zhang, Y. Qi and J. Xiao, *Science*, 2020, **370**, 1313–1317.
6 D. Cantillo, M. Damm, D. Dallinger, M. Bauser, M. Berger and C. O. Kappe, *Org. Process Res. Dev.*, 2014, **18**, 1360–1366.
7 P. Chen, H. Dou, J. Zhang, C. He and S. Pang, *ACS Appl. Mater. Interfaces*, 2023, **15**, 4144–4151.
8 Y. Tang, D. Kumar and J. n. M. Shreeve, *J. Am. Chem. Soc.*, 2017, **139**, 13684–13687.
9 C. Li, H. Li, H.-H. Zong, Y. Huang, M. Gozin, C. Q. Sun and L. Zhang, *iScience*, 2020, **23**, 100944.
10 F. Zhao, C. Zhang, Y. Wang, *et al.*, *ACS Appl. Mater. Interfaces*, 2019, **11**, 35851–35859.
11 H. Chen, T. Zhang and J. Zhang, *J. Hazard. Mater.*, 2009, **161**, 1473–1477.
12 H. Chen, T. Zhang, J. Zhang, X. Qiao and K. Yu, *J. Hazard. Mater.*, 2006, **129**, 31–36.
13 R. Rajak, P. Kumar and S. Dharavath, *Cryst. Growth Des.*, 2024, **24**, 2142–2148.
14 M. Pierce-Butler, *Acta Crystallogr. B*, 1982, **38**, 3097–3100.
15 S. S. Park, Y. Tulchinsky and M. Dincă, *J. Am. Chem. Soc.*, 2017, **139**, 13260–13263.
16 J. S. Rao, T. C. Dinadayalane, J. Leszczynski and G. N. Sastry, *J. Phys. Chem. A*, 2008, **112**, 12944–12953.
17 N. Ding, C. Zhao, J. Zhang, Y. Du, Q. Sun, S. Li and S. Pang, *Adv. Sci.*, 2025, **12**, 2409093.
18 S. Saha, M. K. Mishra, C. M. Reddy and G. R. Desiraju, *Acc. Chem. Res.*, 2018, **51**, 2957–2967.
19 R. Devarapalli, S. B. Kadambi, C.-T. Chen, G. R. Krishna, B. R. Kammari, M. J. Buehler, U. Ramamurty and C. M. Reddy, *Chem. Mater.*, 2019, **31**, 1391–1402.
20 L. R. Redfern and O. K. Farha, *Chem. Sci.*, 2019, **10**, 10666–10679.
21 W. Gui-xiang, S. Chun-hong, G. Xue-dong and X. He-ming, *J. Phys. Chem. A*, 2009, **113**, 1318–1326.
22 H. Yang, S. J. Hwang, H. H. Lee, K. H. Yoo, S. H. Choi, J. H. Lee, J. Y. Park, J. K. Kim, H. S. Kim and W. K. Jang, *J. Am. Chem. Soc.*, 2011, **133**, 19666–19669.
23 H.-Y. Chen, T.-L. Zhang, J.-G. Zhang, L. Yang and X.-J. Qiao, *Chin. J. Chem.*, 2007, **25**, 59–62.
24 L. Wang, H. Chen, T. Zhang, J. Zhang and L. Yang, *J. Hazard. Mater.*, 2007, **147**, 576–580.
25 A. Schoedel, M. Li, D. Li, M. O'Keeffe and O. M. Yaghi, *Chem. Rev.*, 2016, **116**, 12466–12535.
26 K. G. Balachandar and A. Thangamani, *Heliyon*, 2020, **6**, e03163.
27 K. Koner, K. Das, R. P. Paitandi, R. Mahapatra, A. Sarkar, A. Sury, Y. H. Koo, Y. Zhang, T. Heine, A. Kuc, P. P. Pillai, S. Seki, C. M. Reddy and R. Banerjee, *J. Am. Chem. Soc.*, 2025, **147**, 9972–9980.
28 S. Bhunia, S. Chandel, S. K. Karan, S. Dey, A. Tiwari, S. Das, N. Kumar, R. Chowdhury, S. Mondal, I. Ghosh, A. Mondal, B. B. Khatua, N. Ghosh and C. M. Reddy, *Science*, 2021, **373**, 321–327.
29 W. C. Oliver and G. M. Pharr, *J. Mater. Res.*, 2004, **19**, 3–20.
30 G. Pharr and W. Oliver, *J. Mater. Res.*, 1992, **7**, 1564–1583.
31 J.-M. Seo, H.-J. Noh, H. Y. Jeong and J.-B. Baek, *J. Am. Chem. Soc.*, 2019, **141**, 11786–11790.
32 Q. Zhang and J. n. M. Shreeve, *Angew. Chem., Int. Ed.*, 2014, **53**, 2540–2542.
33 M. Jujam, R. Rajak and S. Dharavath, *Adv. Funct. Mater.*, 2025, **35**, 2412638.
34 V. W. Manner, M. J. Cawkwell, K. D. Spielvogel, D. G. Tasker, J. W. Rose, M. Aloi, R. Tucker, J. D. Moore, M. C. Campbell and T. D. Aslam, *J. Am. Chem. Soc.*, 2024, **146**, 26286–26296.
35 (*a*) W. C. Oliver and G. M. Pharr, *J. Mater. Res.*, 2004, **19**, 3–20; (*b*) G. Pharr and W. Oliver, *J. Mater. Res.*, 1992, **7**, 1564–1583.
36 J.-M. Seo, H.-J. Noh, H. Y. Jeong and J.-B. Baek, *J. Am. Chem. Soc.*, 2019, **141**, 11786–11790.
37 (*a*) K. G. Balachandar and A. Thangamani, *Heliyon*, 2020, **6**, e03163; (*b*) S. Dharavath, V. D. Ghule and K. Muralidharan, *New J. Chem.*, 2014, **38**, 3699–3707.
38 (*a*) A. K. Yadav, V. D. Ghule and S. Dharavath, *Mater. Chem. Front.*, 2021, **5**, 8352–8360; (*b*) A. K. Yadav, V. D. Ghule and S. Dharavath, *ACS Appl. Mater. Interfaces*, 2022, **14**, 49898–49908.
39 (*a*) CCDC 2401613: Experimental Crystal Structure Determination, 2025, DOI: **10.5517/ccdc.csd.cc2lm2dq**; (*b*) CCDC 2449186: Experimental Crystal Structure Determination, 2025, DOI: **10.5517/ccdc.csd.cc2n6l0h**; (*c*) CCDC 2449189: Experimental Crystal Structure Determination, 2025, DOI: **10.5517/ccdc.csd.cc2n6l3l**; (*d*) CCDC 2449198: Experimental Crystal Structure Determination, 2025, DOI: **10.5517/ccdc.csd.cc2n6ldw**; (*e*) CCDC 2449208: Experimental Crystal Structure Determination, 2025, DOI: **10.5517/ccdc.csd.cc2n6lq6**; (*f*) CCDC 2449429: Experimental Crystal Structure Determination, 2025, DOI: **10.5517/ccdc.csd.cc2n6tvk**; (*g*) CCDC 2483913: Experimental Crystal Structure Determination, 2025, DOI: **10.5517/ccdc.csd.cc2pcq71**; (*h*) CCDC 2484895: Experimental Crystal Structure Determination, 2025, DOI: **10.5517/ccdc.csd.cc2pdqxr**.